3-бөлім **Раздел 3** **Section 3**

Қолданбалы математика **Прикладная математика** **Applied mathematics**

IRSTI 27.35.45 DOI: https://doi.org/10.26577/JMMCS208110426

S.D. Alpar[1*], F.A. Baktygerey[1], A.M. Aubakirova[1], M.S. Mukaram[1], F.K. Tokmukhamedova[1,2], A.Zh. Ydyrys[1]

[1]International Information Technology University, Almaty, Kazakhstan

[2]La Rochelle University, La Rochelle, France

*e-mail: s.alpar@iitu.edu.kz

OPTIMIZING THE INSULATION LAYER FOR ENERGY EFFICIENCY IN BUILDING FACADES

This paper examines the role of shape optimization in improving the thermal performance of building facades. The study investigates whether modifying the internal interface between brick and expanded polystyrene (EPS) insulation can enhance seasonal thermal performance without increasing material usage. A two-dimensional steady-state heat diffusion model is solved using a finite-difference scheme. The interface is parameterized by a cubic polynomial under a strict volume-preservation constraint, and optimal shapes are determined through a discrete search. Results indicate that interface geometry affects heat transfer differently across seasons: redistribution of insulation changes thermal resistance under summer conditions, while in winter it alters conductive heat pathways. Overall, geometric redistribution can influence seasonal thermal response while keeping total material volume constant. Without insolation, however, the winter-optimal geometry increases heat loss, so the winter result applies to peak-insolation conditions only.

Keywords: shape optimization, building facades, heat transfer, building energy efficiency, finite-difference method.

С.Д. Алпар[1*], Ф.А. Бақтыгерей[1], А.М. Аубакирова[1], М.С. Мұқарам[1], Ф.К. Токмухамедова[1,2], А.Ж. Ыдырыс[1]

[1]Халықаралық ақпараттық технологиялар университеті, Алматы, Қазақстан

[2]Ля Рошель университеті, Ля Рошель, Франция

*e-mail: s.alpar@iitu.edu.kz

Ғимарат қасбеттерінің энергия тиімділігін арттыру үшін жылу оқшаулағыш қабатты оңтайландыру

Бұл жұмыс құрылыс қасбеттерінің жылу тиімділігін арттырудағы пішінді оңтайландырудың рөлін зерттейді. Зерттеудің мақсаты — кірпіш қабаты мен кеңейтілген полистирол (EPS) оқшаулағышы арасындағы ішкі шекараны геометриялық өзгерту арқылы материал көлемін арттырмай-ақ маусымдық жылу сипаттамаларын жақсартуға болатынын анықтау. Осы мақсатта екі өлшемді стационарлық жылу өткізгіштік моделі әзірленіп, ол ақырлы айырымдар әдісімен шешілді. Шекара материал көлемін сақтау шартымен кубтық көпмүшелік арқылы параметрленіп, оңтайлы пішіндер дискретті іздеу әдісімен анықталды. Нәтижелер шекара геометриясының жылу берілісіне маусымға байланысты әсер ететінін көрсетті: жазда оқшаулағыштың қайта бөлінуі жылу кедергісін өзгертеді, ал қыста өткізгіш жылу жолдарын түрлендіреді. Жалпы материал көлемі өзгермеген жағдайда да геометриялық қайта бөлу маусымдық жылу реакциясына әсер ете алатыны анықталды. Алайда күн радиациясы болмаған жағдайда қысқы оңтайлы пішін жылу шығынын арттырады, сондықтан қысқы нәтиже тек күн сәулесінің ең жоғары мәніне сәйкес жағдайға қатысты.

Түйін сөздер: пішінді оңтайландыру, ғимарат қасбеттері, жылу алмасу, ғимараттардың энергия тиімділігі, ақырлы айырымдар әдісі.

© 2026 Al-Farabi Kazakh National University

С.Д. Алпар[1*], Ф.А. Бактыгерей[1], А.М. Аубакирова [1], М.С. Мукарам[1], Ф.К. Токмухамедова[1,2], А.Ж. Ыдырыс[1]
[1]Международный университет информационных технологий, Алматы, Казахстан
[2]Университет Ля Рошели, Ля Рошель, Франция
[*]e-mail: s.alpar@iitu.edu.kz

Оптимизация теплоизоляционного слоя для повышения энергоэффективности фасадов зданий

Данная работа посвящена исследованию роли оптимизации формы в повышении тепловой эффективности строительных фасадов. Цель исследования — опреде-лить, может ли геометрическое изменение внутренней границы между слоем кирпича и утеплителем из пенополистирола (ППС) улучшить сезонные тепловые характеристики без увеличения объёма материалов. Для этого была разработана двумерная стационарная модель теплопроводности, решённая методом конечных разностей. Внутренняя граница параметри-зована кубическим полиномом при строгом сохранении объёма материала, а оптимальные формы определялись методом дискретного поиска. Результаты показывают, что геометрия границы влияет на теплоперенос по-разному в разные сезоны: летом перераспределение утеплителя изменяет тепловое сопротивление, а зимой модифицирует пути теплопроводнос-ти внутри стены. Таким образом, геометрическое перераспределение может влиять на сезон-ный тепловой отклик без изменения общего объёма материала. Однако при отсутствии солнечной радиации зимняя оптимальная форма увеличивает теплопотери, поэтому зимний результат относится только к условиям пиковой инсоляции.
Ключевые слова: оптимизация формы, фасады зданий, теплопередача, энергоэффективность зданий, метод конечных разностей.

1 Introduction

Buildings account for a significant share of global energy consumption and greenhouse gas emissions. According to the International Energy Agency, the building sector is responsible for approximately 30% of global energy use, and energy demand has increased by about 20% since 2019 [1]. Improving building energy efficiency is therefore a key objective of climate policy.

In Kazakhstan, characterized by long cold winters and hot summers, the residential sector alone consumed 33% of total final energy in 2020, slightly more than industry [2]. Kazakhstan adopted the Concept for Transition to a Green Economy [3] and aims to achieve carbon neutrality by 2060 [4]. Improving the thermal performance of building envelopes is therefore an important national priority.

Conventional building physics models typically represent wall assemblies as one-dimensional combinations of flat material layers [5]. Such simplifications neglect two-dimensional heat transfer effects and spatial variations of boundary conditions. Solar radiation on facades can be non-uniform due to shading [6], while convective heat transfer coefficients vary with airflow and facade height [7]. These factors contribute to the performance gap between predicted and actual building energy use [8]. Berger et al. [9] developed a 2D model capturing non-uniform shading and variable convective coefficients, finding substantial differences compared to 1D approaches.

This study investigates the optimization of the internal boundary between a brick layer and expanded polystyrene (EPS) insulation in a multi-layer wall. The interface is parameterized using a cubic polynomial with two parameters controlling amplitude and curvature. A two-dimensional steady-state heat transfer model is applied to evaluate thermal

performance under representative summer and winter solstice conditions for Almaty. The results demonstrate how interface shape affects heat transfer in multi-layer walls and present a performance-based approach to building envelope design [10, 11].

2 Methodology

2.1 Physical domain and governing equation

The physical domain considered in this study is illustrated in Fig. 1.

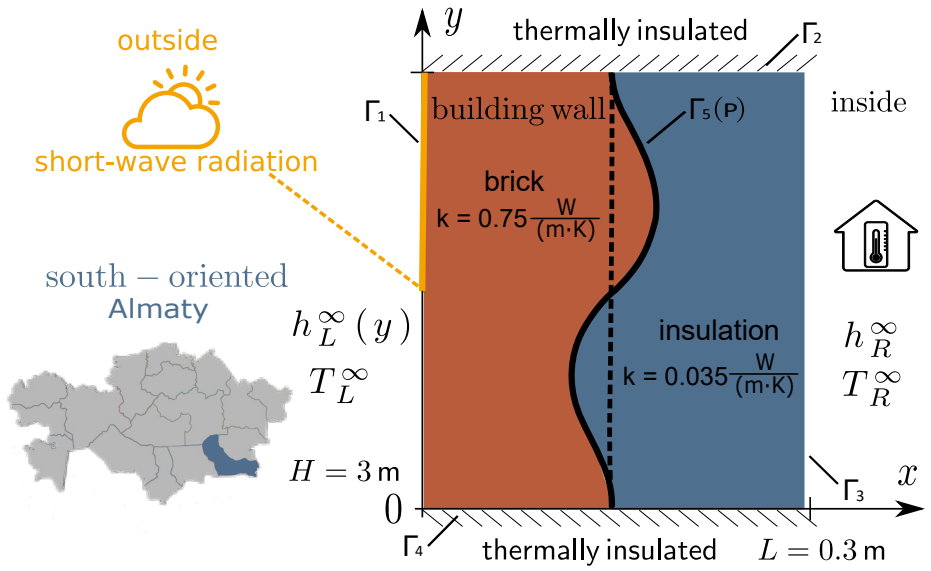


Figure 1: Illustration of the physical domain.

The computational domain Ω is a vertical cross-section of a two-layer building wall with height $H = 3$ m and total thickness $L = 0.3$ m:

$$\Omega = \{(x, y) \in \mathbb{R}^2 : \ 0 < x < L, \ 0 < y < H\},$$

where x is directed perpendicular to the wall plane and y is the vertical coordinate. A two-dimensional formulation is adopted because incident solar radiation and the exterior convective coefficient vary significantly with height due to urban shading and wind-profile effects, which a one-dimensional model cannot capture.

The boundary decomposes as $\partial\Omega = \Gamma_1 \cup \Gamma_2 \cup \Gamma_3 \cup \Gamma_4$: Γ_1 is the exterior surface subject to solar irradiance and convection, Γ_3 is the interior surface, and Γ_2, Γ_4 are thermally adiabatic boundaries.

The wall consists of a brick outer layer ($k_b = 0.75\ \mathrm{W\,m^{-1}K^{-1}}$) and an EPS insulation inner layer ($k_i = 0.035\ \mathrm{W\,m^{-1}K^{-1}}$), separated by an internal interface Γ_5. The ratio $k_b/k_i \approx 21$ means that even a modest redistribution of insulation thickness produces a measurable change in net heat flux — the physical basis of the shape optimization.

Steady-state heat diffusion is governed by:

$$\nabla \cdot \big(k(x, y)\, \nabla T(x, y)\big) = 0, \qquad \forall\, (x, y) \in \Omega, \tag{1}$$

where $k(x, y)$ equals k_b in the brick subdomain and k_i in the insulation subdomain. The steady-state formulation is used to compare interface geometries at two representative instants, the summer and winter solstice at noon, rather than to estimate the energy balance of the wall over a day or a season. The reasons for this choice and the limitations it imposes on the interpretation of the results are discussed in Section 4.4.

2.2 Boundary and interface conditions

On the exterior surface Γ_1, a Robin boundary condition combines outdoor convection with absorbed short-wave solar flux:

$$k\,\nabla T \cdot \mathbf{n} = -h_L^{\infty}(y)\big(T - T_L^{\infty}\big) + q_L^{\infty}(y), \tag{2}$$

where the convective coefficient follows a power-law atmospheric boundary layer profile:

$$h_L^{\infty}(y) = h_0 + h_1 \frac{V_{\infty}}{V_0} \left(\frac{y}{y_0}\right)^{\lambda}, \tag{3}$$

with $h_0 = 5.82\ \mathrm{W\,m^{-2}K^{-1}}$, $h_1 = 3.96\ \mathrm{W\,m^{-2}K^{-1}}$, $\lambda = 0.32$, $V_0 = 1.0\ \mathrm{m\,s^{-1}}$ and $y_0 = 65.33$ m. These coefficients follow the height-dependent convection model of [12], in the form adopted for a facade of the same dimensions in [13]. The quantity y_0 is a reference height of the wind profile rather than a characteristic size of the wall, for $0 < y < 3$ m it yields a moderate variation of h_L^{∞} along the facade, which is the effect the two-dimensional model is meant to capture. The absorbed solar flux is prescribed by the profile

$$q_L^{\infty}(y) = 300\,\tan\!\Big(\frac{\pi}{4}\,\frac{y}{H}\Big) \tag{4}$$

which vanishes at the base of the wall and reaches 300 $\mathrm{W\,m^{-2}}$ at the top. The profile is a simplified representation of a facade whose lower part is shaded by neighbouring buildings, consistent with the non-uniform irradiation patterns reported in [9, 13]. The peak value is based on the Meteonorm irradiation data for Almaty [14], following the approach of [13], where the same database was used for the solar loading of the facade. The same profile is applied to both solstices. This is a deliberate simplification: the solar altitude in Almaty differs strongly between June and December, so the results compare geometries under an identical radiative load rather than reproduce the actual seasonal irradiation. On the interior surface Γ_3:

$$k\,\nabla T \cdot \mathbf{n} = -h_R^{\infty}\big(T - T_R^{\infty}\big), \qquad \forall\,(x, y) \in \Gamma_3, \tag{5}$$

with $h_R^{\infty} = 7\ \mathrm{W\,m^{-2}K^{-1}}$, a value close to the interior surface resistance $R_{si} = 0.13\ \mathrm{m^2K\,W^{-1}}$ given for horizontal heat flow in [15]. The top and bottom boundaries are adiabatic:

$$k\,\nabla T \cdot \mathbf{n} = 0, \qquad \forall\,(x, y) \in \Gamma_2 \cup \Gamma_4.$$

At the internal interface Γ_5, continuity of temperature and normal heat flux is enforced:

$$T\big|_{\gamma-0} = T\big|_{\gamma+0}, \qquad k_b\,\nabla T \cdot \mathbf{n}_5\big|_{\gamma-0} = k_i\,\nabla T \cdot \mathbf{n}_5\big|_{\gamma+0}. \tag{6}$$

2.3 Interface parametrization and constraints

The interface is described by $x = \gamma(p, y)$ via the cubic polynomial:

$$\gamma(p, y) = \frac{L}{2} + p_0\Big(g(y) - S_{\text{shift}}\Big), \qquad g(y) = \frac{y}{H}\left(\frac{y}{H} - p_1\right)\left(\frac{y}{H} - 1\right), \tag{7}$$

where p_0 is the deformation amplitude and has the dimension of length(metres), since the shape function $g(y) - S_{\text{shift}}$ is dimensionless, and $p_1 \in [0, 1]$ is a dimensionless parameter that sets the vertical location of the extrema. This two-parameter family covers convex, concave, and S-shaped profiles. The shift term

$$S_{\text{shift}} = \frac{1}{H}\int_0^H g(y)\, dy = \frac{2p_1 - 1}{12} \tag{8}$$

enforces the material-preservation constraint:

$$\frac{1}{H}\int_0^H \gamma(p, y)\, dy = \frac{L}{2}, \tag{9}$$

so any improvement comes purely from geometric redistribution of a fixed insulation volume. The interface is further required to stay inside the wall with a margin δ_L from both surfaces,

$$\delta_L \le \gamma(p, y) \le L - \delta_L, \qquad \forall\, y \in [0, H], \tag{10}$$

with $\delta_L = 0.25L = 0.075$ m, the spatial tolerance used for the same cubic parametrization in [13]. Condition (10) bounds p_0 to $\left[p_0^{\min}(p_1),\, p_0^{\max}(p_1)\right]$ and keeps each material layer at least 0.075 m thick.

2.4 Numerical solution

The boundary value problem is solved by a finite-difference method on a uniform Cartesian grid with spacings $\Delta x = L/(N_x - 1)$, $\Delta y = H/(N_y - 1)$. Conductivity discontinuities at the interface are handled through harmonic averaging of face conductivities:

$$k_E = \frac{2k_{j,i}\, k_{j,i+1}}{k_{j,i} + k_{j,i+1}}, \quad k_W = \frac{2k_{j,i}\, k_{j,i-1}}{k_{j,i} + k_{j,i-1}}, \quad k_N = \frac{2k_{j,i}\, k_{j+1,i}}{k_{j,i} + k_{j+1,i}}, \quad k_S = \frac{2k_{j,i}\, k_{j-1,i}}{k_{j,i} + k_{j-1,i}},$$

which reproduces the exact flux through a cell face shared by two materials in series. Arithmetic averaging would overestimate the face conductivity by the factor $(k_b{+}k_i)^2/(4k_bk_i)$, which equals about 5.9 for the present pair of materials and grows with the ratio k_b/k_i. The discrete balance at interior nodes is:

$$a_P\, T_{j,i} = a_E\, T_{j,i+1} + a_W\, T_{j,i-1} + a_N\, T_{j+1,i} + a_S\, T_{j-1,i},$$

with $a_E = k_E/\Delta x^2$, $a_W = k_W/\Delta x^2$, $a_N = k_N/\Delta y^2$, $a_S = k_S/\Delta y^2$, $a_P = a_E + a_W + a_N + a_S$.

The interface curve $\gamma(p, y)$, restricted to $[\delta_L,\, L{-}\delta_L]$, is approximated by a cubic smoothing spline, sampled at the grid rows and filtered with a Gaussian kernel of width $\sigma = 1$ grid step

in y, i.e. from 15 mm on the 101×201 grid to 3.75 mm on the 401×801 grid. The filter suppresses spurious oscillations of the staircase interface near the conductivity jump, since its width is tied to the grid step, the smoothing vanishes under refinement. Each node is then assigned to brick or insulation according to its position relative to the filtered interface. The system is solved by the Successive Over-Relaxation (SOR) method with the relaxation parameter

$$\omega = \frac{2}{1 + \sin(\pi/m)}, \qquad m = \max(N_x,\, N_y),$$

and the stopping criterion $\|T^{(k)} - T^{(k-1)}\|_\infty \leq \varepsilon = 10^{-8}$, where k is the iteration number. SOR serves only as the linear solver for the discrete system; the accuracy of the discretization itself is assessed separately in Section 2.5.

2.5 Verification

The implementation was verified in two steps. First, a manufactured-solution benchmark was solved for the Helmholtz equation $\Delta u + 3u = f$ on $\Omega = [0, 0.25] \times [0, 0.5]$ with the exact solution $u_{\text{exact}} = \sin(x + 2y) + e^{2x+3y}$, Dirichlet conditions on three sides and a Neumann condition on the bottom boundary. The discrete system was solved by the Jacobi, Gauss–Seidel and SOR iterations. As shown in Fig. 2, the maximum-norm error decreases as $\mathcal{O}(h^2)$ for all three solvers and is the same for each of them, since they converge to the same discrete solution and differ only in the number of iterations. The numbers of iterations are given in Table 1: SOR requires one to two orders of magnitude fewer iterations than the Jacobi and Gauss–Seidel methods and is therefore used as the linear solver in the optimization.

Table 1: Number of iterations required by the Jacobi, Gauss–Seidel and SOR methods on different grids.

Grid $N_x \times N_y$	Jacobi	Gauss–Seidel	SOR
11×21	442	374	**81**
21×41	2324	1286	**171**
51×101	8046	6830	**443**
101×201	59311	24306	**897**
201×401	158700	85860	**1806**
301×601	318496	178547	**2714**
512×1024	831000	462263	**4634**

Second, for a flat interface with constant h_L^∞ and q_L^∞, the problem reduces to one-dimensional conduction through two layers in series, for which

$$Q_{\text{an}} = H\, \frac{T_L^\infty + q_L^\infty / h_L^\infty - T_R^\infty}{1/h_L^\infty + L/(2k_b) + L/(2k_i) + 1/h_R^\infty}. \tag{11}$$

With $h_L^\infty = 10\ \mathrm{W\,m^{-2}K^{-1}}$, $q_L^\infty = 150\ \mathrm{W\,m^{-2}}$, $T_L^\infty = -5\,^\circ\mathrm{C}$ and $T_R^\infty = 20\,^\circ\mathrm{C}$, Eq. (11) gives $Q_{\text{an}} = -6.344\ \mathrm{W\,m^{-1}}$. The computed flows are compared with this value in Table 2: the relative deviation halves with each refinement.

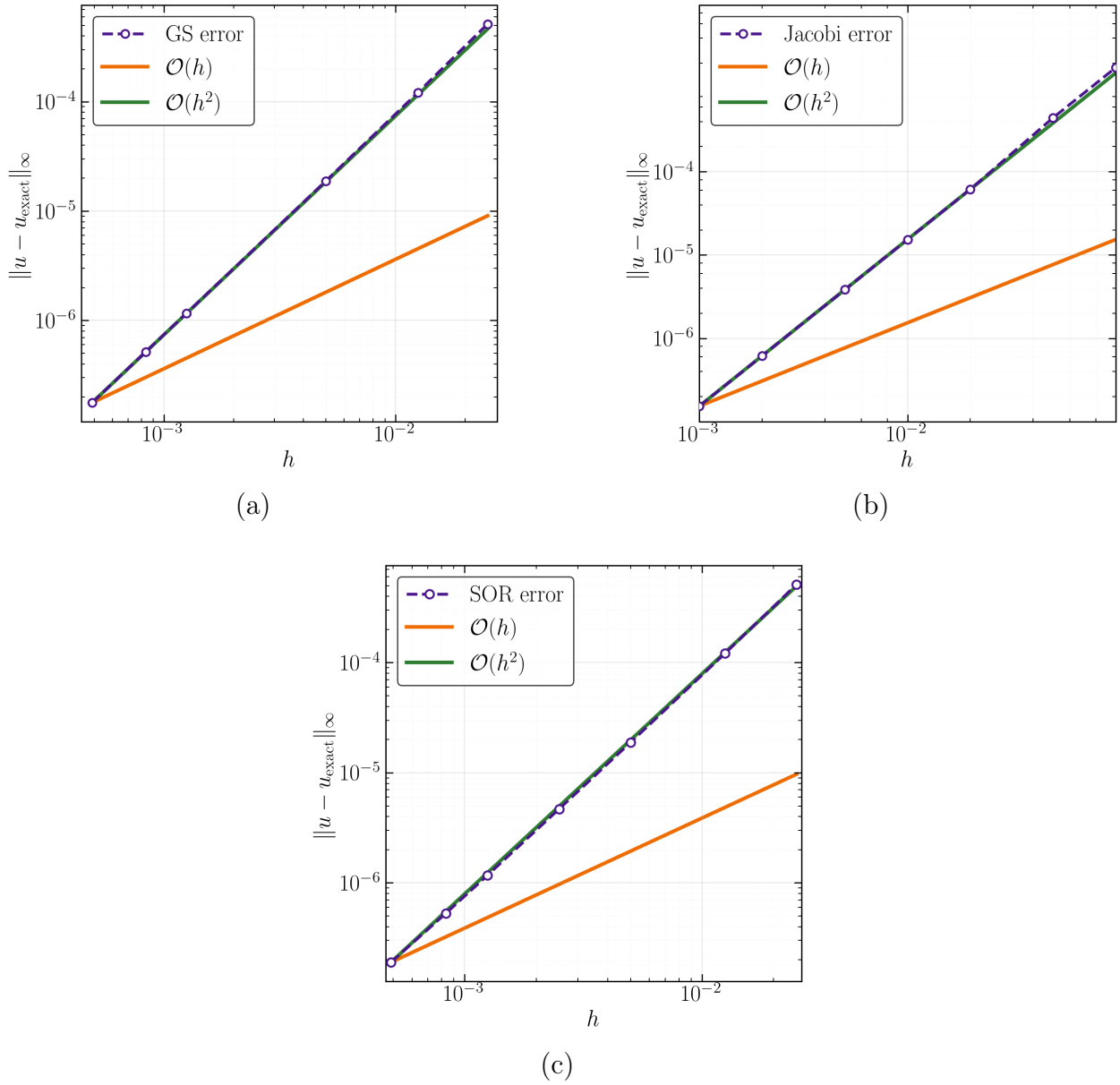


Figure 2: The convergence behaviour of the three iterative solvers is illustrated in panels (a), (b), and (c), which correspond to the Gauss–Seidel, Jacobi, and Successive Over-Relaxation (SOR) methods, respectively.

Table 2: Flat wall with constant h_L^∞ and q_L^∞: computed flow and deviation from the analytical value $Q_{\text{an}} = -6.344$ W/m

Grid	Q_{num} (W/m)	Relative deviation (%)
101×201	-6.290	0.86
201×401	-6.317	0.43
401×801	-6.331	0.22

The flat-wall solution converges with first order, in contrast to the second order observed in the manufactured-solution benchmark. The flat interface $x = L/2$ coincides with a column of grid nodes, and these nodes are assigned to the insulation layer, so the effective insulation thickness is larger than the nominal one by half a grid spacing, and the brick layer is thinner by the same amount. With an insulation thickness of $L/2 + \Delta x/2$ and a brick thickness of $L/2 - \Delta x/2$, Eq. (11) gives -6.290, -6.317 and $-6.331\ \mathrm{W\,m^{-1}}$, which coincide with the numerical values in Table 2; this geometric effect therefore accounts for the first-order convergence. The physical model itself was not validated against experimental data.

3 Optimization problem

The performance indicator is the total inward convective heat flow at Γ_3:

$$Q_s(p) = \int_0^H h_R^{\infty}\big(T(L, y, p) - T_{R,s}^{\infty}\big)\, dy, \qquad s \in \{\mathrm{sum}, \mathrm{win}\}, \tag{12}$$

evaluated via the trapezoidal rule. In summer a positive Q_{sum} is an unwanted heat gain that adds to the cooling load, so it is minimized. In winter the objective is the opposite: Q_{win} is maximized, i.e. the geometry that lets the largest part of the absorbed solar energy reach the interior surface is sought. This is a maximization of passive solar gains, it coincides with a reduction of heat losses only under the fixed insolation of the steady-state problem and does not hold at night or under overcast conditions. Both objectives are unified through the sign convention:

$$\mathcal{J}_s(p) = \sigma_s\, Q_s(p), \qquad \sigma_{\mathrm{sum}} = +1, \quad \sigma_{\mathrm{win}} = -1, \tag{13}$$

so both seasons share the same minimization form:

$$p_s^{\star} = \arg\min_{p \in \Omega_p} \mathcal{J}_s(p), \qquad s \in \{\mathrm{sum}, \mathrm{win}\}. \tag{14}$$

The material-preservation constraint (9) is satisfied automatically for all $p \in \Omega_p$, so any change of Q_s is attributable solely to geometric redistribution of the fixed insulation volume. Since $\mathcal{J}_s$ is not guaranteed to be convex over Ω_p, seasonal optima are identified by exhaustive discrete search. The parameter p_1 takes 51 uniformly spaced values in $[0, 1]$ ($\Delta p_1 = 0.02$); for each p_1, p_0 takes 25 uniformly spaced values between $p_0^{\min}(p_1)$ and $p_0^{\max}(p_1)$, so the step in p_0 depends on p_1. The flat interface $p_0 = 0$ is added to this set whenever it does not coincide with one of the 25 values; owing to round-off, this occurs for 30 of the 51 values of p_1. One search over Ω_p thus requires $51 \times 25 + 30 = 1305$ evaluations of the objective function; it was carried out for each season on each grid.

4 Case study

The case study considers a brick–EPS composite wall in Almaty, Kazakhstan, under two peak-load regimes: the summer solstice (June 21) and the winter solstice (December 21). The same wall geometry and governing equations as in Section 2 were used: $H = 3\,\mathrm{m}$, $L = 0.3\,\mathrm{m}$, brick on the exterior side, and EPS insulation on the interior side. For each season, the flat

interface $x = L/2$ was compared with the optimized interface generated by Eq. (7). Since the volume-preservation constraint is enforced through Eq. (8), both configurations contain the same amount of insulation. The material properties are listed in Table 3.

Table 3: Thermal conductivity of the materials

Material	k (W/m·K)
Brick	0.75
Expanded polystyrene	0.035

The seasonal boundary parameters are given in Table 4. The exterior and interior boundary conditions follow Eqs. (2)–(5), with height-dependent convection and solar loading defined by Eqs. (3) and (4). The objective quantity is the inward convective heat flow $Q_s(p)$ in Eq. (12), minimized in summer and maximized in winter according to Eq. (13).

Table 4: Seasonal boundary parameters used in the case study

Regime	T_L^∞ (°C)	T_R^∞ (°C)	V_∞ (m/s)
Summer (June 21)	35	20	3.0
Winter (December 21)	−5	20	3.0

4.1 Admissible Design Space

The internal interface was described by $x = \gamma(p, y)$ with the design vector $p = (p_0, p_1)$, as defined in Eq. (7). The parameter p_0 controls the deformation amplitude, while p_1 determines the vertical position of the extrema. The admissible domain Ω_p was obtained from the geometric feasibility and volume-preservation constraints described in Section 2. The resulting design region is shown in Fig. 3. The horizontal axis gives the amplitude parameter p_0 in metres, and the vertical axis the dimensionless position parameter p_1.

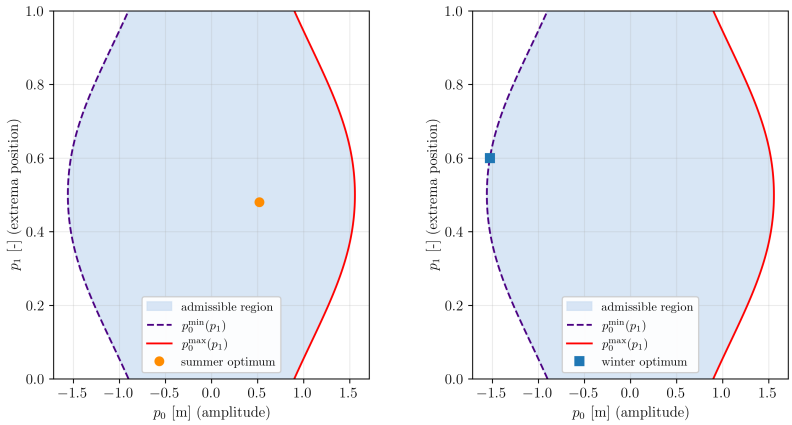


Figure 3: Admissible design region Ω_p with the summer optimum (left) and the winter optimum (right), the winter optimum lies on the lower bound $p_0^{\min}(p_1)$.

The shaded region in Fig. 3 contains all admissible parameter pairs. The feasible range of p_0 depends on p_1, so the search domain is not rectangular. Therefore, the discrete optimization was restricted to the admissible set Ω_p.

4.2 Results

The flat and optimized interfaces were compared for both seasonal regimes using Q_s as the main performance indicator. The optimized temperature fields are shown in Fig. 4, while interface shapes, heat-flux profiles, and temperature profiles are compared in Fig. 5.

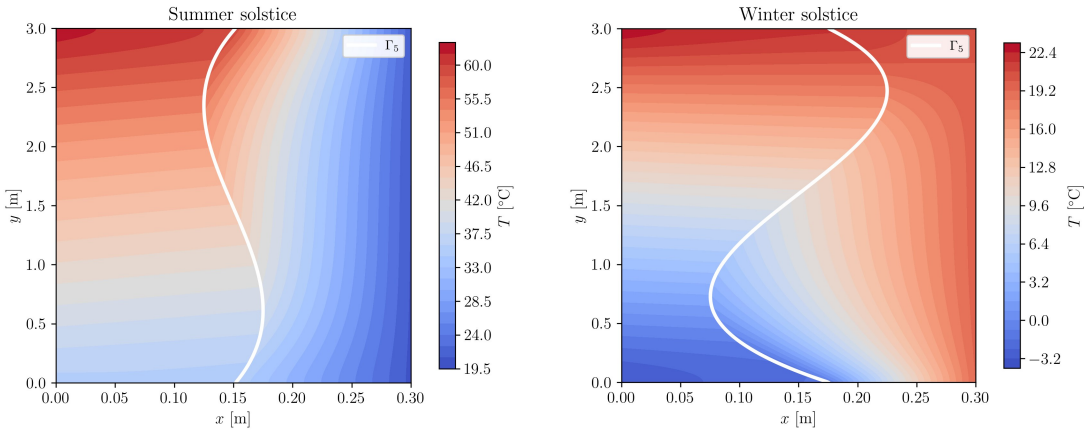


Figure 4: Temperature distributions with the optimized interface for the summer (a) and winter (b) solstice cases.

Summer solstice. For the summer solstice, $\mathcal{J}_{\text{sum}}(p) = Q_{\text{sum}}(p)$ was minimized according to Eq. (13). The results on three grids are given in Table 5. On the finest grid, Q_{sum} decreased from 18.167 to 17.969 W m^{-1}, i.e. by 0.198 W per metre of wall length. The optimum lies inside the admissible domain, at $p_0 \approx 0.52$ and $p_1 = 0.48$ on the two finer grids. As shown in Fig. 5, the optimized interface shifts insulation toward the upper solar-loaded region.

Table 5: Flat and optimized interface, summer solstice

Grid	$Q_{\text{sum}}^{\text{flat}}$ (W/m)	$Q_{\text{sum}}^{\text{opt}}$ (W/m)	ΔQ (W/m)	p_0 (m)	p_1
101×201	18.04930	17.96806	−0.08124	0.519	0.52
201×401	18.12730	17.96860	−0.15870	0.519	0.48
401×801	18.16655	17.96880	−0.19775	0.519	0.48

Winter solstice. For the winter solstice, $\sigma_{\text{win}} = -1$ was used in Eq. (13), so that Q_{win} was maximized. The results are given in Table 6. Under the prescribed conditions the absorbed solar flux does not compensate the transmission loss, and Q_{win} is negative for both geometries, i.e. heat leaves the room. On the finest grid the optimized interface reduces this net loss from 7.104 to 6.410 W m^{-1}, a change of +0.694 W per metre of wall length. The optimum, $p_0 \approx -1.526$, $p_1 = 0.60$, coincides with the lower bound $p_0^{\min}(p_1)$ of the admissible domain: the gain is limited by the minimum insulation thickness δ_L of Eq. (10) rather than by an interior extremum of the objective. As shown in Figs. 4(b) and 5, the optimized interface leaves a

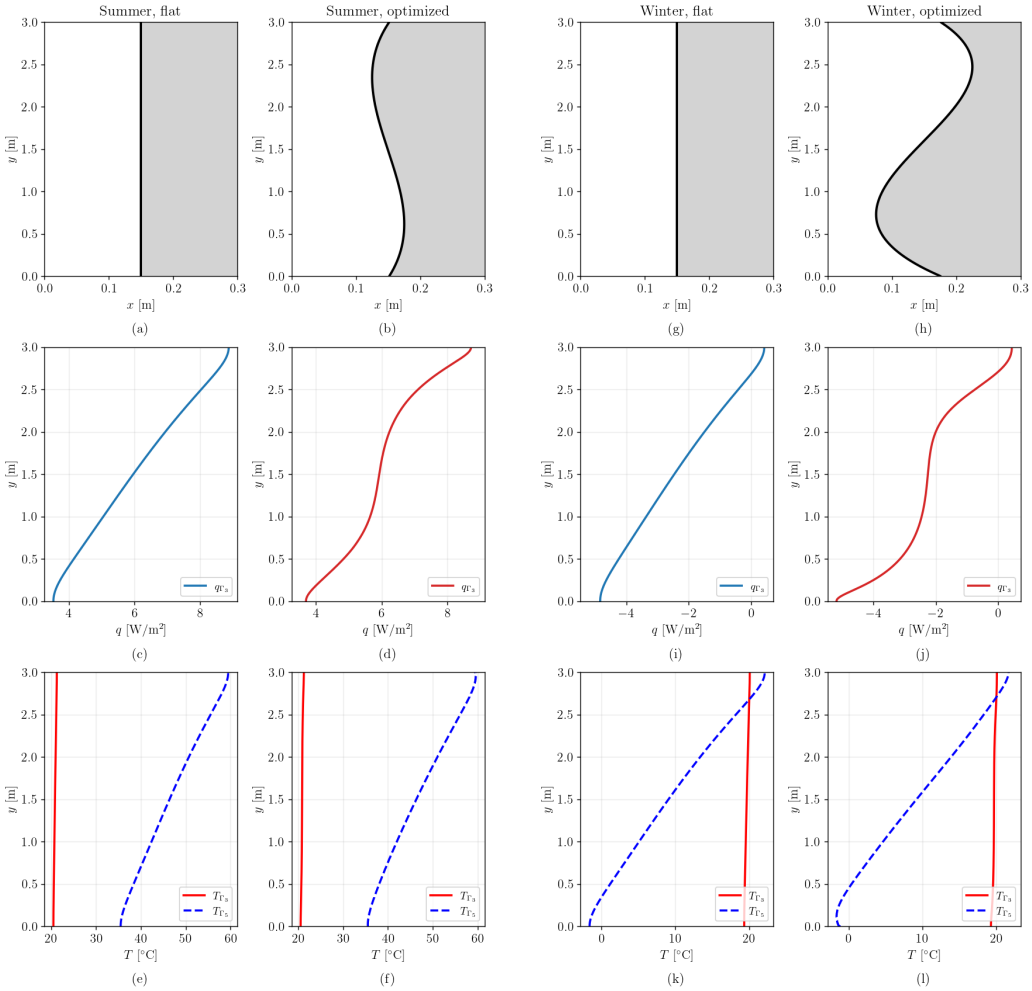


Figure 5: Comparison of flat and optimized interfaces in summer, panels (a)–(f), and in winter, panels (g)–(l). In each season the left column shows the flat interface and the right column the optimized one. Summer: flat (a, c, e) and optimized (b, d, f), winter: flat (g, i, k) and optimized (h, j, l). Rows from top to bottom: interface geometry (brick on the left, EPS in grey), panels (a), (b), (g), (h), inward heat flux at Γ_3, panels (c), (d), (i), (j), temperatures at Γ_3 and Γ_5, panels (e), (f), (k), (l).

conductive brick pathway in the upper solar-loaded region, through which absorbed heat reaches the interior surface. This gain exists only while the facade is irradiated (Section 4.4).

Table 6: Flat and optimized interface, winter solstice

Grid	$Q_{\text{win}}^{\text{flat}}$ (W/m)	$Q_{\text{win}}^{\text{opt}}$ (W/m)	ΔQ (W/m)	p_0 (m)	p_1
101×201	-7.05911	-6.41061	$+0.64850$	-1.538	0.58
201×401	-7.08876	-6.41030	$+0.67846$	-1.526	0.60
401×801	-7.10368	-6.41004	$+0.69364$	-1.526	0.60

The seasonal optima are therefore physically different: the summer geometry increases local shielding, whereas the winter geometry preserves a conductive pathway in the solar-

loaded region. The spatial arrangement of the same insulation volume thus affects the two-dimensional thermal response of the wall.

4.3 Mesh convergence

The grids in Tables 5 and 6 are refined with a constant ratio of 2. The observed order of convergence p and the extrapolated value Q_{ext} were estimated by Richardson extrapolation,

$$p = \frac{\ln\left|(Q_2 - Q_1)/(Q_3 - Q_2)\right|}{\ln 2}, \qquad Q_{\mathrm{ext}} = Q_3 + \frac{Q_3 - Q_2}{2^p - 1},$$

where indices 1–3 denote the coarse, medium and fine grids. The results are summarized in Table 7.

Table 7: Observed order of convergence and extrapolated values

Quantity	p	Q_{ext} (W/m)
$Q^{\mathrm{flat}}_{\mathrm{sum}}$	0.99	18.206
ΔQ_{sum}	0.99	−0.238
$Q^{\mathrm{flat}}_{\mathrm{win}}$	0.99	−7.119
ΔQ_{win}	0.98	+0.709

The flat-wall flows and the seasonal differences ΔQ converge with first order, in agreement with the verification of Section 2.5. As shown there, the flat interface lies on a column of grid nodes assigned to the insulation, which makes the insulation layer effectively thicker by $\Delta x/2$ and reduces $|Q^{\mathrm{flat}}|$ on coarse grids. The optimized flows, in contrast, change by less than $8 \cdot 10^{-4}$ W m^{-1} between the three grids in both seasons and are practically grid-independent; no convergence order is reported for them. Most of the grid dependence of ΔQ therefore comes from the flat-wall solution, whose magnitude increases with grid refinement. In summer, ΔQ changes from -0.081 to -0.198 W m^{-1} and tends to about -0.24 W m^{-1}; in winter, it changes from $+0.649$ to $+0.694$ W m^{-1} and tends to about $+0.71$ W m^{-1}. The remaining discretization error on the finest grid, estimated as $|Q_{\mathrm{ext}} - Q_3|$, is about 0.04 W m^{-1} in summer and 0.015 W m^{-1} in winter for both Q^{flat} and ΔQ, which is several times smaller than the seasonal effects. The extrapolated values are therefore taken as the main estimates of the seasonal effects. In both seasons, the optimal parameters (p_0, p_1) are identical on the two finer grids. On the coarsest grid, p_1 differs by one or two search steps (in winter p_0 changes accordingly, since the bound $p_0^{\min}$ depends on p_1), while the optimal value of the objective changes by less than $8 \cdot 10^{-4}$ W m^{-1}, i.e. the objective is nearly flat around its minimum.

4.4 Limitations of the steady-state formulation

The optima reported above correspond to two instants of peak solar load and do not describe the performance of a static wall over a day or a year. The winter geometry shows this most clearly. The brick pathway that carries absorbed solar energy inwards at noon also lowers the local thermal resistance of the wall. To quantify this, the flat interface and the winter-optimal interface of the 201×401 grid were recomputed with $q_L^{\infty} = 0$ and all other winter conditions unchanged. Without insolation the heat loss is 15.760 W m^{-1} for the flat interface

and 17.679 $\mathrm{W\,m^{-1}}$ for the optimized one, i.e. the optimized geometry loses 1.919 $\mathrm{W\,m^{-1}}$ more. This is almost three times the gain of 0.678 $\mathrm{W\,m^{-1}}$ obtained at noon on the same grid. At night and on overcast days, which make up a large part of the winter period in Almaty, the winter-optimal geometry is therefore unfavourable, and the winter result should be read as a property of the peak-insolation regime only.

A transient formulation would remove this restriction, but two problems remain open for shape optimization of building walls. The first concerns the objective function. Indicators proposed in the literature rely on the indoor–outdoor temperature difference or on the time-integrated heat flux at the interior surface [16]. A time-integrated flux measures how much energy passes through the wall, yet it does not separate a useful gain during a sunny winter day from an unwanted loss during the following night, and the phase lag between outdoor conditions and the flux delivered to the room is not taken into account [13]. A criterion suited to alternating heating and cooling demand has to be defined first. The second problem is computational: exhaustive search needs one solution of the heat equation per candidate shape, and with a transient solver each of them turns into a simulation over the whole period of interest. Building simulation tools are also poorly adapted to geometric design variables and mostly rely on parametric or lumped steady-state representations of the envelope [17,18].

The model is purely thermal. With the insulation on the interior side, the dew point moves towards the masonry, which may cause interstitial condensation, coupled heat and moisture transfer was not considered. Since the summer and winter optima are opposite, a single fixed interface cannot be optimal for both seasons, and an annual criterion based on a transient model evaluated jointly over the heating and cooling periods is needed.

Regarding practical realization, a curved brick–insulation interface of the amplitudes considered here is not standard masonry practice. Additive manufacturing of walls offers one possible route: the first 3D-printed house in Central Asia was completed in Almaty in 2024, with printed concrete walls insulated by expanded polystyrene concrete [19]. A simpler option is to keep a flat load-bearing layer and vary only the thickness of the insulation boards, for instance with CNC-cut EPS elements. Another option for future work is to keep the internal layers flat and modify only the external shell of the facade, as in [13], which is easier to construct. Cost and constructibility of these options were outside the scope of this study.

5 Conclusion

The effect of the shape of the internal interface between a brick layer and an EPS layer on the heat flow through a two-layer wall was studied with a two-dimensional steady-state heat conduction model. The interface was described by a two-parameter cubic polynomial with a fixed insulation volume and a minimum layer thickness of $0.25L$, the equation was discretized by finite differences with harmonic averaging of the conductivity, the linear system was solved by the SOR method, and the optimal shapes were found by exhaustive search. The implementation was verified against a manufactured solution and against the one-dimensional analytical solution for a flat wall, with a relative error of 0.22% on the finest grid.

For the summer solstice, the optimized interface reduced the inward heat flow by about 0.24 $\mathrm{W\,m^{-1}}$ according to Richardson extrapolation (0.198 $\mathrm{W\,m^{-1}}$ on the finest grid); the remaining discretization error is several times smaller than this difference. For the winter

solstice at noon, the optimized interface reduced the net heat loss by about 0.71 $\mathrm{W\,m^{-1}}$ (0.694 $\mathrm{W\,m^{-1}}$ on the finest grid) with the same insulation volume, by keeping a conductive brick pathway in the solar-loaded upper part of the wall. This optimum lies on the boundary of the admissible domain and is set by the minimum insulation thickness δ_L: a smaller δ_L enlarges the admissible set and cannot decrease the winter gain. Without insolation, the same winter geometry loses 1.92 $\mathrm{W\,m^{-1}}$ more than the flat wall.

The two seasonal optima have opposite shapes, and the winter result holds only under peak insolation. Conclusions about the annual energy performance of a wall with a fixed curved interface cannot be drawn from the present model. Future work will address a transient formulation evaluated jointly over the heating and cooling periods, coupled heat and moisture transfer, and the constructability of the resulting geometries.

Authors contribution. S.A.: conceptualization, methodology, supervision, writing – original draft preparation. **F.T., A.Y.**: formal analysis, investigation, writing – original draft preparation. **F.B., A.A., M.S.**: validation, writing – review and editing. **F.B., A.A., M.S.**: methodology, writing – review and editing. All authors have read and agreed to the published version of the manuscript.

Acknowledgments. This research is funded by the Science Committee of the Ministry of Science and Higher Education of the Republic of Kazakhstan (Grant No. AP32318683).

References

[1] International Energy Agency. 2025. "Energy Efficiency 2025." IEA, Paris. https://www.iea.org/reports/energy-efficiency-2025.

[2] International Energy Agency. 2022. "Kazakhstan 2022: Energy Sector Review." IEA, Paris. https://www.iea.org/reports/kazakhstan-2022.

[3] President of the Republic of Kazakhstan. 2013. "Concept for Transition of the Republic of Kazakhstan to a Green Economy." Decree No. 577.

[4] Government of the Republic of Kazakhstan. 2020. "Kazakhstan's commitment to achieve carbon neutrality by 2060." Official statement.

[5] Ürge-Vorsatz, Diana, Luisa F. Cabeza, Susana Serrano, Camila Barreneche, and Ksenia Petrichenko. 2015. "Heating and cooling energy trends and drivers in buildings." Renewable and Sustainable Energy Reviews 41: 85-98.

[6] Allegrini, Jonas, Viktor Dorer, and Jan Carmeliet. 2012. "Influence of the urban microclimate in street canyons on the energy demand for space cooling and heating of buildings." Energy and Buildings 55: 823–832.

[7] Mirsadeghi, M., Daniel Cóstola, B. Blocken, and Jan Hensen. 2013. "Review of external convective heat transfer coefficient models in building energy simulation programs: Implementation and uncertainty." Applied Thermal Engineering 56: 134–151.

[8] Pieter de Wilde. 2014. "The gap between predicted and measured energy performance of buildings: A framework for investigation." Automation in Construction 41: 40-49.

[9] Berger, Julien, Suelen Gasparin, Walter Mazuroski, and Nathan Mendes. 2021. "An efficient two-dimensional heat transfer model for building envelopes." Numerical Heat Transfer, Part A: Applications 79 (3): 163–194. https://doi.org/10.1080/10407782.2020.1836936.

[10] K. Martin, A. Erkoreka, I. Flores, M. Odriozola, and J.M. Sala. 2011. "Problems in the calculation of thermal bridges in dynamic conditions." Energy and Buildings 43 (2): 529-535.

[11] Lauzet, Nicolas, Auline Rodler, Marjorie Musy, Marie-Hélène Azam, Sihem Guernouti, Dasaraden Mauree, and Thibaut Colinart. 2019. "How building energy models take the local climate into account in an urban context – A review." Renewable and Sustainable Energy Reviews 116: 109390.

[12] McAdams, W. H.. 1985. Heat Transmission. Krieger Pub Co.

[13] Alpar, Sultan, Julien Berger, Walter Mazuroski, and Rafik Belarbi. 2024. "Shape optimization of the energy efficiency of building retrofitted facade." Solar Energy 271: 112437.

[14] Meteonorm Software. 2020. "Global climate database."

[15] International Organization for Standardization. 2017. "ISO 6946:2017 Building components and building elements – Thermal resistance and thermal transmittance – Calculation methods."

[16] Barrios, G., G. Huelsz, J. Rojas, J. M. Ochoa, and I. Marincic. 2012. "Envelope wall/roof thermal performance parameters for non air-conditioned buildings." Energy and Buildings 50: 120–127.

[17] Caetano, Inês, Luís Santos, and António Leitão. 2020. "Computational design in architecture: Defining parametric, generative, and algorithmic design." Frontiers of Architectural Research 9 (2): 287-300.

[18] Ekici, B., C. Cubukcuoglu, M. Turrin, and I. S. Sariyildiz. 2019. "Performative computational architecture using swarm and evolutionary optimisation: A review." Building and Environment 147: 356–371.

[19] COBOD International. 2024. "First 3D printed house in Central Asia constructed to withstand earthquakes of 7 on the Richter scale." https://cobod.com/first-3d-printed-house-in-central-asia-constructed-to-withstand-earthquakes-of-7-on-the-richter-scale/.

Information about authors:

Alpar Sultan Duisenuly – PhD, Associate Professor at the International Information Technology University (Almaty, Kazakhstan, email: s.alpar@iitu.edu.kz).

Baktygerey Fatima Aybekkyzy – bachelor at the International Information Technology University (Almaty, Kazakhstan, email: 34141@iitu.edu.kz).

Aubakirova Altynay Mahabbatkyzy – bachelor at the International Information Technology University (Almaty, Kazakhstan, email: 34114@iitu.edu.kz).

Mukaram Madiyar Sabyrzhanuly – bachelor at the International Information Technology University (Almaty, Kazakhstan, email: 34456@iitu.edu.kz).

Tokmukhamedova Fatima Kadyrovna – master, assistant-professor at the International Information Technology University (Almaty, Kazakhstan, email: f.tokmukhamedova@iitu.edu.kz).

Ydyrys Aizhan Zhumabaykyzy – PhD, Associate Professor at the International Information Technology University (Almaty, Kazakhstan, email: a.ydyrys@iitu.edu.kz).

Авторлар туралы мәлімет:

Алпар Султан Дуйсенұлы – PhD, Халықаралық ақпараттық технологиялар университетінің қауымдастырылған профессоры (Алматы, Қазақстан, электрондық пошта: s.alpar@iitu.edu.kz).

Бақтыгерей Фатима Айбекқызы – Халықаралық ақпараттық технологиялар университетінің бакалавры (Алматы, Қазақстан, электрондық пошта: 34141@iitu.edu.kz).

Аубакирова Алтынай Махаббатқызы – Халықаралық ақпараттық технологиялар университетінің бакалавры (Алматы, Қазақстан, электрондық пошта: 34114@iitu.edu.kz).

Мұқарам Мадияр Сабыржанұлы – Халықаралық ақпараттық технологиялар университетінің бакалавры (Алматы, Қазақстан, электрондық пошта: 34456@iitu.edu.kz).

Токмухамедова Фатима Кадыровна – магистр, Халықаралық ақпараттық технологиялар университетінің ассистент-профессоры (Алматы, Қазақстан, электрондық пошта: f.tokmukhamedova@iitu.edu.kz).

Ыдырыс Айжан Жұмабайқызы – PhD, Халықаралық ақпараттық технологиялар университетінің қауымдастырылған профессоры (Алматы, Қазақстан, электрондық пошта: a.ydyrys@iitu.edu.kz).

Информация об авторах:

Алпар Султан Дуйсенулы – PhD, ассоциированный профессор Международного университета информационных технологий (Алматы, Казахстан, электронная почта: s.alpar@iitu.edu.kz).

Бактыгерей Фатима Айбеккызы – бакалавр Международного университета информационных технологий (Алматы, Казахстан, электронная почта: 34141@iitu.edu.kz).

Аубакирова Алтынай Махаббаткызы – бакалавр Международного университета информационных технологий (Алматы, Казахстан, электронная почта: 34114@iitu.edu.kz).

Мукарам Мадияр Сабыржанулы – бакалавр Международного университета информационных технологий (Алматы, Казахстан, электронная почта: 34456@iitu.edu.kz).

Токмухамедова Фатима Кадыровна – магистр, ассистент-профессор Международного университета информационных технологий (Алматы, Казахстан, электронная почта: f.tokmukhamedova@iitu.edu.kz).

Ыдырыс Айжан Жумабайкызы – PhD, ассоциированный профессор Международного университета информационных технологий (Алматы, Казахстан, электронная почта: a.ydyrys@iitu.edu.kz).

Revised: June 6, 2026
Accepted: November 14, 2026